TISSUE ENGINEERING: Part A
Volume 20, Numbers 23 and 24, 2014

DOI: 10.1089/ten.tea.2013.0694

Passive Strain-Induced Matrix Synthesis and Organization in Shape-Specific, Cartilaginous Neotissues

Regina F. MacBarb, PhD,[1] Nikolaos K. Paschos, MD, PhD,[1,2] Reedge Abeug, BS,[1] Eleftherios A. Makris, MD, PhD,[1,3] Jerry C. Hu, PhD,[1] and Kyriacos A. Athanasiou, PhD, PE[1,4]

Tissue-engineered musculoskeletal soft tissues typically lack the appropriate mechanical robustness of their native counterparts, hindering their clinical applicability. With structure and function being intimately linked, efforts to capture the anatomical shape and matrix organization of native tissues are imperative to engineer functionally robust and anisotropic tissues capable of withstanding the biomechanically complex *in vivo* joint environment. The present study sought to tailor the use of passive axial compressive loading to drive matrix synthesis and reorganization within self-assembled, shape-specific fibrocartilaginous constructs, with the goal of developing functionally anisotropic neotissues. Specifically, shape-specific fibrocartilaginous neotissues were subjected to 0, 0.01, 0.05, or 0.1 N axial loads early during tissue culture. Results found the 0.1-N load to significantly increase both collagen and glycosaminoglycan synthesis by 27% and 67%, respectively, and to concurrently reorganize the matrix by promoting greater matrix alignment, compaction, and collagen cross-linking compared with all other loading levels. These structural enhancements translated into improved functional properties, with the 0.1-N load significantly increasing both the relaxation modulus and Young's modulus by 96% and 255%, respectively, over controls. Finite element analysis further revealed the 0.1-N uniaxial load to induce multiaxial tensile and compressive strain gradients within the shape-specific neotissues, with maxima of 10.1%, 18.3%, and −21.8% in the *XX*-, *YY*-, and *ZZ*-directions, respectively. This indicates that strains created in different directions in response to a single axis load drove the observed anisotropic functional properties. Together, results of this study suggest that strain thresholds exist within each axis to promote matrix synthesis, alignment, and compaction within the shape-specific neotissues. Tailoring of passive axial loading, thus, presents as a simple, yet effective way to drive *in vitro* matrix development in shape-specific neotissues toward more closely achieving native structural and functional properties.

Introduction

Musculoskeletal soft tissues support body movement by withstanding complex mechanical loads, with each tissue having morphological and mechanical characteristics specific to its biomechanical role. Failure or degeneration of a single tissue in a diarthrodial joint can lead to functional impairment of the entire joint. Unfortunately, current treatment modalities often fail to fully restore joint functionality.[1] Tissue engineering has therefore garnered increasing interest over the last decade as a means to generate clinically relevant musculoskeletal implants. A potential advantage of this approach is to generate neotissues with specific characteristics that are necessary for withstanding the mechanical complexity of joints. Given that the highly specialized biomechanical roles of musculoskeletal soft tissues are closely related to their matrix organization,[2] it has become of critical importance to capture the anisotropic functionality of native tissues during *in vitro* neotissue development.

Mechanical stimulation has shown efficacy in driving the biomechanical characteristics of engineered tissues.[3–9] Natively, musculoskeletal soft tissues are subjected to loading during all phases of their lifespan. Importantly, loading is critical to the development, maturation, and maintenance of their mechanical integrity.[10–14] Efforts to identify beneficial biomechanical stimuli have focused on determining efficacious loading types (e.g., compressive, tensile, hydrostatic

[1]Department of Biomedical Engineering, University of California, Davis, Davis, California.
[2]Department of Trauma and Orthopaedic Surgery, Orthopaedic Sports Medicine Center of Ioannina, University of Ioannina, Ioannina, Greece.
[3]Department of Orthopedic Surgery and Musculoskeletal Trauma, University of Thessaly (BIOMED), Larisa, Greece.
[4]Department of Orthopedic Surgery, Lawrence Ellison Center for Tissue Regeneration and Repair, School of Medicine, University of California, Davis, Sacramento, California.

pressure, and shear) and regimens (e.g., static versus dynamic, durations, resting periods, and magnitudes). While stimuli have been successful in increasing some functional characteristics of engineered tissues, their properties remain far from reaching native tissue values, particularly in an anisotropic manner. It is, therefore, necessary that the effect of loading on neotissue development be more carefully assessed to fine-tune its use toward engineering clinically robust neotissues with anisotropic characteristics necessary to perform their intended biomechanical role.

With structure and function being intimately linked, a key criterion for engineering functionally anisotropic constructs is that they attain a native-like matrix organization. To achieve this goal, several studies have developed anatomically shaped matrix scaffolds made of either natural or synthetic fibers, or even the two combined.[15–18] Such scaffolds, however, have been found to exhibit insufficient biomechanical integrity, particularly in the case of naturally derived fibers.[19,20] Scaffolds also suffer from biodegradability and biocompatibility issues, as especially seen with synthetic scaffolds.[21–23] Further, it has been suggested that use of any scaffolding material may hinder both cellular communication and responsiveness to external stresses.[24] Such drawbacks have led to the development of a scaffold-free, self-assembling process to cartilage and fibrocartilage tissue engineering.[24,25] In this method, high densities of cells are seeded into nonadherent wells, where they quickly coalesce and, over time, produce a robust matrix in a manner akin to native morphogenesis.[26] Further, self-assembled neotissue has been readily formed into several complex, clinically relevant shapes, such as the knee meniscus[27] and temporomandibular joint (TMJ) disc.[28] While these anatomically shaped neotissues have been found to exhibit mechanical properties that are at times on par with native tissues, they still lack the overall anisotropic functionality and biomechanical integrity of their native tissue counterparts.

Mechanical strain has been shown to result in fiber alignment within collagen-rich neotissues.[29–32] For example, engineered vessels subjected to circumferential strain during an 8-week culture period exhibited highly organized matrices capable of withstanding pressures up to 2000 mmHg (267 kPa).[33] Similarly, in ligament tissue engineering, axial mechanical strain was found to induce uniaxial collagen alignment and anisotropic functional properties.[31] It has also been shown that self-assembling fibrocartilaginous neotissues around a central post guides development of circumferential collagen fiber organization.[27] Together, such work indicates that mechanical strain can be strategically tailored to promote matrix reorganization toward engineering more functionally robust neotissues.

Recently, the concept of using strain to improve matrix organization has been investigated in self-assembled TMJ disc neotissues. In this study, biconcave neotissues were subjected to a 1 g mass (0.01-N load) early during development.[28] The significance of this study was that neotissue loaded with 1 g had tensile properties trending higher than unweighted controls; however, the 1.1–2% strains induced by this load were insufficient to cause detectable changes in collagen organization. This study further found that the 1 g of mass was unable to promote the neotissue to capture the anisotropic functional trends of the native TMJ disc. The present study, therefore, aimed to tailor the use of different levels of passive axial compression to trigger region-specific collagen reorganization within self-assembled, TMJ disc-shaped neotissues. Overall, it was hypothesized that a strain threshold exists to drive matrix synthesis and alignment within the biconcave constructs, leading to the development of functionally anisotropic neotissues.

Materials and Methods

Cell isolation

Articular chondrocytes (ACs) and meniscus cells (MCs) were harvested from juvenile bovine knee joints (Research 87, Boston, MA), as previously described.[34] Isolated cells were frozen in freezing medium comprising Dulbecco's modified Eagle's medium (DMEM), 20% fetal bovine serum, and 10% dimethyl sulfoxide until cell seeding.

Self-assembly into shape-specific neotissue

Using cocultures of MCs and ACs, biconcave, TMJ-disc-shape-specific constructs were self-assembled as previously described.[28] Briefly, at $t = 0$ day, 50:50 of MC:AC coculture suspensions were seeded into shape-specific 2% agarose wells at 12 M cells/well to induce the formation of biconcave neotissues displaying a thin, inner middle zone surrounded by a thicker, outer band region (Fig. 1A). Shape-specific agarose top pieces were placed on top of the constructs at $t = 3$ days to fully confine their geometry; the constructs remained confined for the remainder of culture. Agarose/construct assemblies were placed in six-well culture plates and fed 6 mL of chondrogenic medium consisting of DMEM, 1% penicillin/streptomycin/fungizone, 1% nonessential amino acids, 100 nM dexamethasone (Sigma, St. Louis, MO), 1% ITS + (BD Scientific, Franklin Lakes, NJ), 40 $\mu g \cdot mL^{-1}$ L-proline, 50 $\mu g \cdot mL^{-1}$ ascorbate-2-phosphate, and 100 $\mu g \cdot mL^{-1}$ sodium pyruvate (Fischer Scientific, Pittsburgh, PA), every other day. At $t = 5$ weeks, constructs were removed from culture and analyzed regionally for their properties.

Passive axial compression of shape-specific constructs

The present study imparted axial compressive loading via 4.75-mm-diameter, type 304 stainless steel posts machined to weigh 1, 5, or 10 g, corresponding to 0.01, 0.05, and 0.1 N loads, respectively. Posts were applied to the shape-specific constructs from $t = 10$ to 14 days based on previous work identifying this time as a critical window in which self-assembled neotissue is most responsive to mechanical stimulation.[35,36] To ensure proper medium diffusion under the post as well as to maintain the tissue's biconcavity, the posts were positioned perpendicular to top of the shape-specific agarose top pieces, such that they were aligned in the center of the neotissue middle zone, as previously described.[28]

Quantitative biochemistry and high-performance liquid chromatography

At $t = 5$ weeks, wet weights of samples designated for biochemical analysis were taken, after which samples were lyophilized and their dry weights were recorded. Following papain digestion,[37] total collagen content was measured using a chloramine-T hydroxyproline assay with a SIRCOL

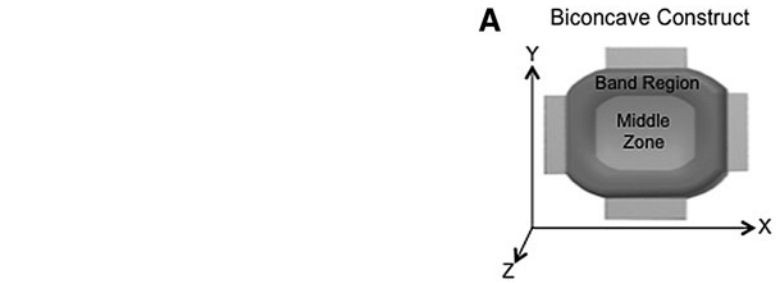

B

	Control	1g	5g	10g
Gross Morphology	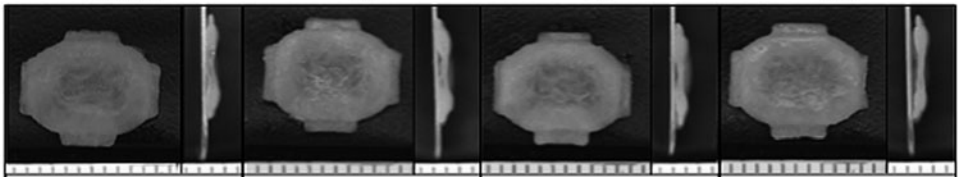			
Major Diameter (mm)	9.4 ± 0.3^{A}	9.4 ± 0.3^{A}	9.2 ± 0.4^{A}	9.2 ± 0.2^{A}
Minor Diameter (mm)	5.3 ± 03^{B}	5.6 ± 0.3^{AB}	5.6 ± 0.3^{AB}	5.9 ± 0.2^{A}
Band Zone Thickness (mm)	0.8 ± 0.1^{A}	0.8 ± 0.1^{A}	0.8 ± 0.1^{A}	0.8 ± 0.1^{A}
Middle Zone Thickness (mm)	0.6 ± 0.2^{A}	0.5 ± 0.1^{AB}	0.5 ± 0.1^{AB}	0.3 ± 0.1^{B}
Band Zone Hydration (%)	92.0 ± 0.7^{A}	90.7 ± 1.4^{A}	91.0 ± 0.5^{A}	90.8 ± 0.5^{A}
Middle Zone Hydration (%)	93.3 ± 1.0^{A}	93.5 ± 0.9^{A}	91.9 ± 1.3^{AB}	91.0 ± 0.8^{B}

FIG. 1. Schematic of biconcave construct indicating the band region and middle zone **(A)**. Gross morphology and growth metrics of neotissue at $t = 5$ weeks **(B)**. Shape-specific neotissue was subjected to 1, 5, or 10 g mass, corresponding to 0.01, 0.05, and 0.1 N loads, respectively, from $t = 10$ to 14 days. Values marked with different letters within each category are significantly different ($p < 0.05$), with A > B > C. Markings on the morphology images are 1 mm apart.

collagen assay standard (Accurate Chemicals, Westbury, NY). A dimethylmethylene blue dye-binding assay kit (Biocolor, Newtownabbey, United Kingdom) was used to measure sulfated glycosaminoglycan (GAG) content. Pyridinoline (PYR) collagen crosslinks were analyzed and quantified via high-performance liquid chromatography (HPLC) using PYR standards (Quidel, San Diego, CA), as previously described.[38,39]

Histology and immunohistochemistry

HistoPrep (Fisher Chemical, Vernon Hills, IL) was used to freeze samples, which were sectioned at 12 μm. Slides were then fixed in formalin before being stained with Safranin O/Fast Green to examine GAG distribution and with Picrosirius Red for total collagen content. Separately, slides were fixed in chilled acetone for collagen types I and II immunohistochemistry (IHC) as previously described.[34]

Stress-relaxation compressive testing

Neotissue compressive properties were measured via uniaxial unconfined stress-relaxation compression testing.[28] Briefly, 2-mm biopsy punches were taken from both the middle zone and band region of the biconcave neotissue. Following height detection, samples were preconditioned for 15 cycles at 5% strain at 1 Hz, after which they were compressed at a strain rate of 1% of the sample height per second to both 10% and 20% strains. Matlab (Mathworks, Natick, MA) was used to fit the resulting data to an equation that assumes that the tissue behaves as Kelvin solid model (Eq. 1).[40] In Equation 1, specimen height (z) and time of strain event (t_i) were determined *a priori*. Deformation (u), time (t), and stress (σ) were recorded during testing. Relaxation modulus (E_r), relaxation time constant (τ_ε), and creep time constant (τ_σ) could be approximated from model fits and then converted into relaxation and instantaneous moduli.[40]

$$\sigma(t) = \sum_{i=1}^{n} \left[\frac{3}{2} \frac{E_r (u_i - u_{i-1})}{z} \left\{ 1 + \left(\frac{\tau_\sigma}{\tau_\varepsilon} - 1 \right) e^{\left(\frac{-(t - t_i)}{\tau_\varepsilon} \right)} \right\} \right] \quad (1)$$

Uniaxial tensile testing

Neotissue tensile properties were obtained from dog-bone samples of the middle zone in the *Y*-direction and of the band region in the *X*-direction using a uniaxial testing machine (Test Resources, Shakopee, MN).[28] For middle-zone samples, dog-bones were ~7.0 mm in total length and 0.5 mm in width at the thinnest point, while band region dog-bone samples were ~5.5 mm in total length and 0.5 mm in width at

the thinnest point. Dog-bone-shaped samples were glued at their extremities to a paper frame, which was clamped into the machine grips. Using a 50-N load cell, a strain-to-failure test was then run at a 1% of the gauge length (measured as the distance between the glued ends of the paper frame) per second. For each sample, the Young's modulus (E_Y) was calculated as the slope of the linear region of the stress–strain curve, while the ultimate tensile strength (UTS) was determined as the curve's peak.

Finite-element analysis

Three-dimensional, computational models of the biconcave neotissue were developed via Autodesk Inventor (Autodesk, San Rafael, CA). Using ABACUS/CAE (Dassault Systèmes, Vélizy-Villacoublay, France), material properties were set to match estimated $t = 10$-day functional properties of the neotissue, as previously described.[28] Specifically, the neotissue was modeled using a 4-noded linear tetrahedral mesh consisting of 52,636 elements. The resulting biconcave model was confined in the *Z*-direction along its bottom surface to represent the axial constraint of the agarose well, while the construct remained free to move in both the *X*- and *Y*-directions to mimic the ability of the neotissue to expand and contract in the wells. A linear, elastic model was used to measure the biconcave model's response to each passive axial loading level (1, 5, and 10 g) once it had fully relaxed to the respective load. The loads were modeled as a pressure distribution across the middle zone of the top surface of the biconcave model. For each load, the resulting stress, strain, and displacement were displayed as a heat map.

Scanning electron microscopy

Samples were dehydrated in increasing ethanol and stored in 70% ethanol at 4°C. Just prior to imaging, samples were transferred into 100% ethanol, dehydrated in a critical point dryer, and gold sputter-coated. Each sample was imaged in three separate locations within their middle zones using a Philips XL30 TMP scanning electron microscope. To quantify scanning electron microscopy (SEM) images, ImageJ was used to measure both fibril density and diameter as previously described.[41] Fibril alignment was quantified using the ImageJ plugin OrientationJ.[42] Ten uniformly sized regions of interest were randomly selected from an overlain grid on SEM images of the neotissue middle zones, from which the software then calculated the corresponding alignment in terms of a coherency factor. Six middle-zone images were analyzed this way for each loading level. The coherency factor, which indicates the degree of local orientation, is an index between 0 and 1. A coherency of 1 corresponds to perfectly oriented and aligned fibrils, while a coherency of 0 refers to completely unoriented fibrils.

Statistical analysis

To determine whether the different passive axial compressive loads resulted in significant changes in neotissue functional and structural properties, a one-way ANOVA ($n = 8$ per group) was used. If the one-way ANOVA showed significance ($p < 0.05$), then a Tukey's Honestly Significant Difference (HSD) *post hoc* test was then applied. All data are represented as mean ± standard deviation (SD), with bars or groups marked by different letters to represent significant differences. For structure-function relationships, results are presented in terms of the coefficient of determination R^2, with positive correlations depicted graphically as positive sloping regression lines, and negative correlations depicted graphically as negative sloping regression lines. Correlations are considered significant at $p < 0.05$.

Results

Gross morphology and growth metrics

While neotissue constructs from all groups maintained the shape-specific biconcavity throughout the entire culture duration, loading level was found to significantly affect construct morphology (Fig. 1B). Specifically, although the major diameter (as measured along the *x*-axis between the outside edges of the band region) was not altered by any of the loading levels, the minor diameter (as measured along the *y*-axis between the outside edges of the band region) of 10-g-loaded constructs was significantly greater than that of controls. Further, while the band region thickness did not change with the different loads, the middle zone of 10-g-loaded constructs was half as thick as the middle zone of controls. In terms of water content, there were no significant differences in whole-construct wet weight or band region hydration among groups. The middle zone of the 10-g-loaded constructs, however, displayed significantly decreased hydration compared with controls.

Quantitative biochemistry and HPLC

Construct collagen, GAG, and PYR contents were measured in both the band and middle-zone regions at $t = 5$ weeks (Fig. 2). No significant differences in collagen per wet weight (Col/WW), GAG per wet weight (GAG/WW), PYR per wet weight (PYR/WW), or PYR per collagen content (PYR/Col) were found among the band regions of any of the groups. While no significant differences in collagen or GAG content were detected among control, 1-g-, or 5-g-loaded constructs in their respective middle zones, the 10 g mass significantly increased both middle-zone Col/WW and GAG/WW by 27% and 67%, respectively, over those of controls. Further, both PYR/WW and PYR/Col were found to be significantly greater in the middle zone of 10-g-loaded constructs, with values 6.8- and 5.2-fold, respectively, those of controls.

Histology and IHC

Representative images of histological and IHC-stained middle-zone samples are shown in Figure 3. Corroborating the biochemical results, similar collagen and GAG staining was observed in the middle zone of control, 1-g-, and 5-g-loaded constructs, while the 10-g mass prompted denser collagen and GAG staining in this region. Collagen I IHC staining became denser with increasing load. Collagen II staining, on the other hand, appeared to slightly decrease in intensity with increasing load.

Stress-relaxation compressive testing

Compressive testing at $t = 5$ weeks found both 10% and 20% strain levels to yield similar trends among the groups;

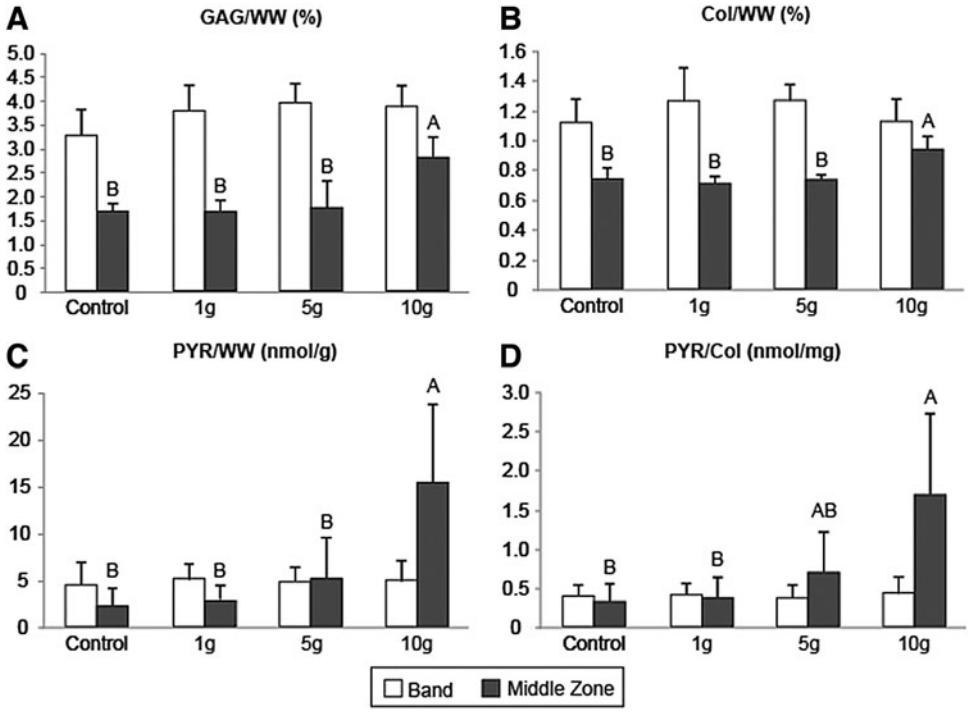

FIG. 2. Glycosaminoglycan per wet weight (GAG/WW) **(A)**, collagen per wet weight (Col/WW) **(B)**, pyridinoline per wet weight (PYR/WW) **(C)**, and PYR per collagen (PYR/Col) **(D)** of biconcave constructs at $t = 5$ weeks. Shape-specific neotissue was subjected to 1-, 5-, or 10-g mass, corresponding to 0.01-, 0.05-, and 0.1-N loads, respectively, from $t = 10$ to 14 days. The 10-g mass promoted significant increases in terms of all four parameters **(A–D)** within the neotissue's middle zone over values achieved in the middle zone of controls; no differences were observed in the neotissue's band region at any loading level. Bars not connected by the same letter are significantly different ($p < 0.05$).

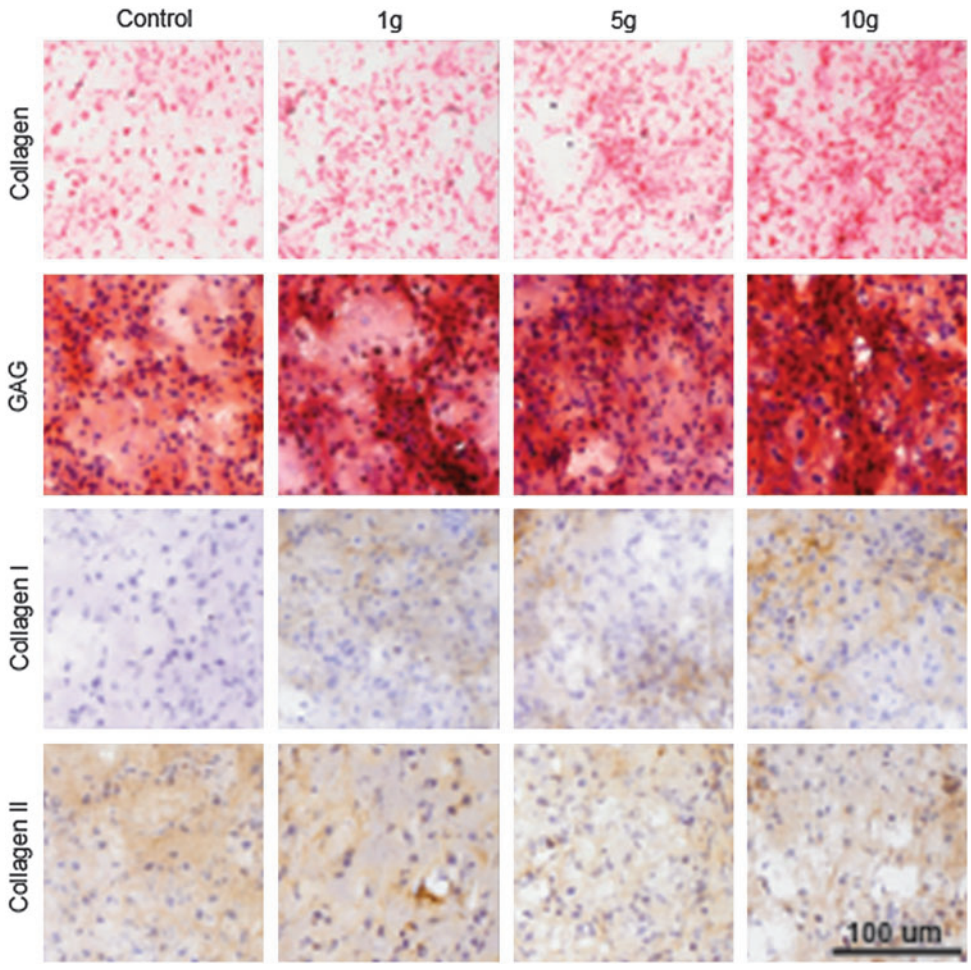

FIG. 3. Histology and immunohistochemistry (IHC) of the middle zone of biconcave neotissue at $t = 5$ weeks. Shape-specific neotissue was subjected to 1-, 5-, or 10-g mass, corresponding to 0.01-, 0.05-, and 0.1-N loads, respectively, from $t = 10$ to 14 days. Collagen was stained using Picrosirius Red and GAG was stained using Safranin O/Fast Green, while IHC was used to stain for collagen types I and II. Denser collagen and GAG staining was observed in 10-g-loaded constructs compared with all other groups. While collagen type I staining increased with increasing load, collagen type II staining appeared to slightly decrease with increasing load. Scale bar is 100 μm for both histology and IHC images. Color images available online at www.liebertpub.com/tea

therefore, only the 20% strain level results are presented (Fig. 4A, B). No significant differences in either the E_r or E_i were found among the band regions of any of the constructs or among the middle zone of control, 1-g-, or 5-g-loaded constructs. The 10 g mass, however, caused a significant increase in both the E_r and E_i in the middle zone by $\sim$96% and 145%, respectively, over the middle zone of all other groups.

Uniaxial tensile testing

Similar to compressive results, uniaxial tensile testing revealed no significant differences in the band region of any constructs in terms of either the E_Y or UTS (Fig. 4C, D). In terms of the middle zone, while the 1-g-loaded constructs trended higher in terms of both the E_Y and UTS compared with controls, the 5-g mass prompted a significant increase in the middle-zone tensile properties over controls. The 10-g-loaded constructs, on the other hand, resulted in significantly greater tensile properties in the middle zone compared with all other groups, exhibiting a 255% and 273% increase in the E_Y and UTS, respectively, over those of controls.

Finite-element analysis

Finite-element analysis (FEA) was conducted to understand the distribution of stresses and strains imparted by passive axial loading in the shape-specific neotissue once it had fully relaxed under an elastic response; thus, it should be noted that the model does not take into account tissue maturation during loading but rather it highlights a snapshot in time to quantify stress and strain distributions. It should be noted that the 4.75-mm-diameter posts used to impart the passive axial loading fit within the middle zone of the neotissue, and therefore modeling of the biconcave, engineered neotissue in response to 1-, 5-, and 10-g masses resulted in the development of different strain distributions and magnitudes localized within the model's middle zone, as seen in Figure 5. For all loading situations, tensile strains were $\sim 1.6\times$ greater in the *YY*-direction compared with the *XX*-direction, while compressive strains were observed only in the *ZZ*-direction. Comparing among loads, maximum strains imparted by the 10-g mass were 9.2-, 10.1-, and 9.9-fold greater than maximum strains achieved by 1 g in the *XX*-, *YY*-, and *ZZ*-directions, respectively. The 5-g mass, on the other hand, increased *XX*-, *YY*-, and *ZZ*-maximum strains by 4.6-, 5.1-, and 5.0-fold over respective maxima achieved by the 1 g mass in each direction.

Scanning electron microscopy

SEM images of construct middle-zone regions were quantified for fibril diameter, density, and alignment at $t = 5$ weeks (Fig. 6). Middle-zone matrix density was found to be significantly greater in constructs loaded with 10 g, with values 1.3-fold those of all other groups. The 10-g mass was further found to significantly enhance fibril diameter in the neotissue's middle zone 1.2-fold that of controls. In terms of alignment, fibrillar coherency in the middle zone was found to be significantly greatest in constructs loaded with 10 g compared with all other groups, with fibrils aligning predominantly in the *Y*-direction.

Structure-function relationships

Neotissue middle-zone Col/WW, GAG/WW, PYR/Col, collagen fibril alignment, and collagen fibril density were correlated with both the E_r and E_Y values (Fig. 7). All correlations were found to be positive and statistically significant. In terms of the middle-zone compressive modulus, strong positive correlations were found with PYR/Col ($R^2 = 0.64$), GAG/WW ($R^2 = 0.53$), and collagen fibril density ($R^2 = 0.55$). Collagen fibril alignment ($R^2 = 0.41$) and Col/WW ($R^2 = 0.44$) demonstrated weak positive correlations with the compressive modulus. For the middle-zone tensile

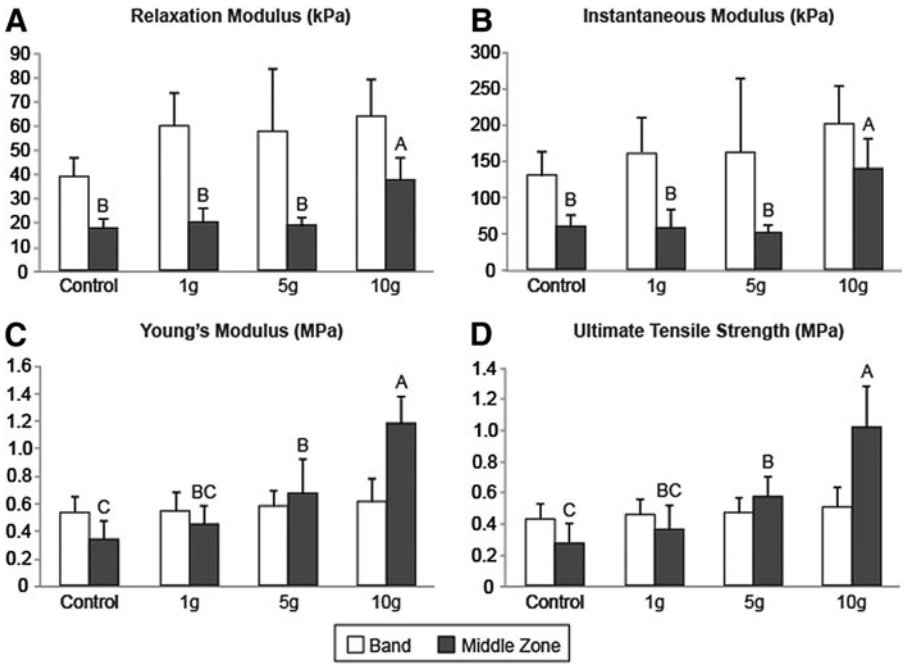

FIG. 4. Relaxation modulus **(A)**, instantaneous modulus **(B)**, Young's modulus **(C)**, and ultimate tensile strength **(D)** of biconcave constructs at $t = 5$ weeks. Shape-specific neotissue was subjected to 1-, 5-, or 10-g mass, corresponding to 0.01-, 0.05-, and 0.1-N loads, respectively, from $t = 10$ to 14 days. The 10-g mass promoted significant increases in terms of all four parameters **(A–D)** within the neotissue's middle zone over values achieved in the middle zone of controls; no differences were observed in the neotissue's band region at any loading level. Bars not connected by the same letter are significantly different ($p < 0.05$).

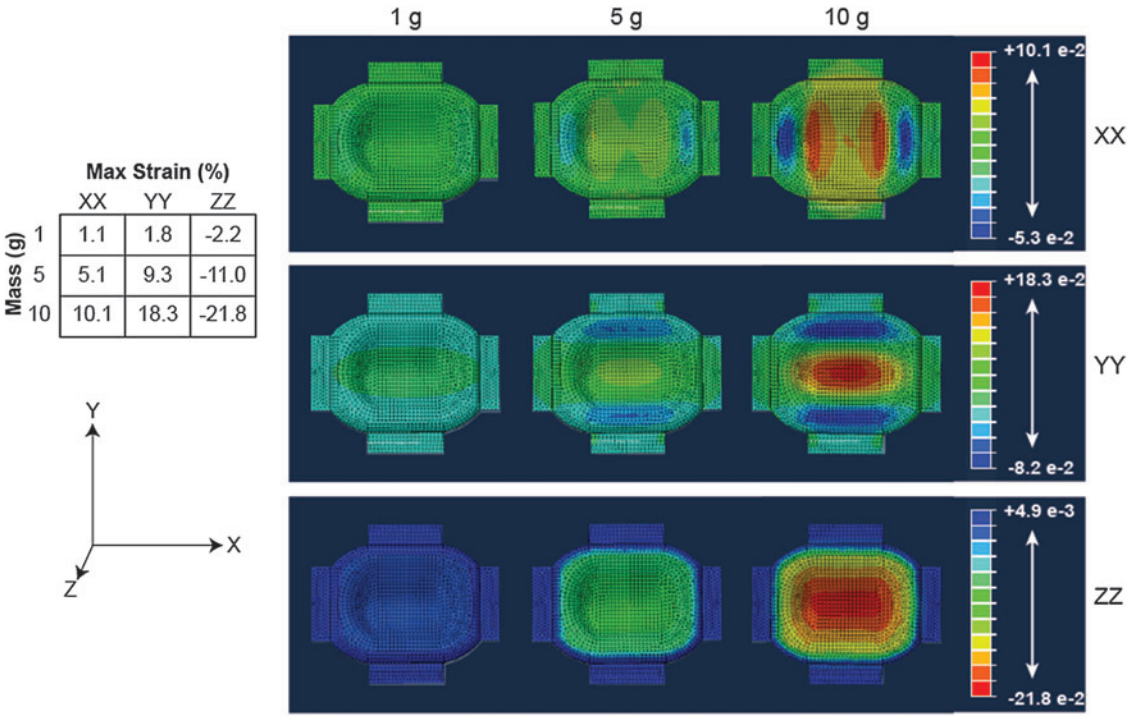

FIG. 5. Strain distributions of three-dimensional computer-aided design (CAD) renderings of biconcave constructs in the *XX*-, *YY*-, and *ZZ*-directions after being subjected to a 1-, 5-, or 10-g mass, corresponding to a 0.01-, 0.05-, and 0.1-N load, respectively. CAD models were developed using a 4-noded linear tetrahedral mesh of 52,636 elements with material properties set to match estimated $t = 10$-day neotissue functional properties. Nodes at the bottom of the model were constrained in the *Z*-direction, and the passive axial load was modeled as a pressure distribution across an area of 54 mm^2 on the top surface of the model. Maximum strains induced by each loading level in each axial direction are provided in the table to the left. Color images available online at www.liebertpub.com/tea

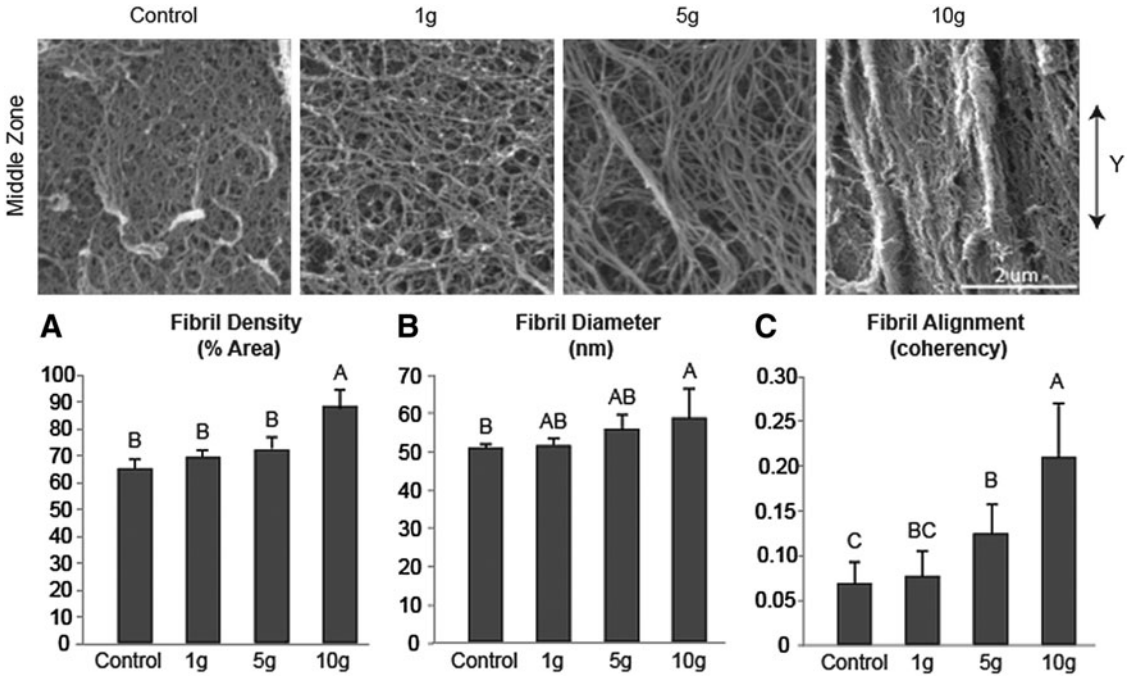

FIG. 6. SEM images taken in the middle zone of biconcave constructs at $t = 5$ weeks (top). Shape-specific neotissue was subjected to 1-, 5-, or 10-g mass, corresponding to 0.01-, 0.05-, and 0.1-N loads, respectively, from $t = 10$ to 14 days. Fibril density **(A)**, fibril diameter **(B)**, and fibril alignment **(C)** were analyzed from SEM images at $t = 5$ weeks. Results found the 10-g mass to promote significant increases in terms of all three parameters **(A–C)** within the neotissue's middle zone over values achieved in the middle zone of controls. Further, the 10-g mass promoted fibrils to align predominantly in the *Y*-direction of the construct middle zone. Bars not connected by the same letter are significantly different ($p < 0.05$). Scale bar is 2 μm.

modulus, the highest strong correlation was with collagen fibril alignment ($R^2 = 0.75$), followed by PYR/Col ($R^2 = 0.64$) and Col/WW ($R^2 = 0.54$), while weak correlations were found with collagen fibril density ($R^2 = 0.42$) and GAG/WW ($R^2 = 0.38$).

Discussion

The objective of this study was to tailor the use of passive axial compression to drive both region-specific matrix synthesis and reorganization toward enhancing the functional properties of shape-specific, engineered fibrocartilage. Results found the 10 g mass to fulfill this objective, as it prompted significantly increased structural and functional properties in the biconcave neotissue's middle zone, while the band region remained unaltered, leading to the development of functionally anisotropic constructs. Specifically, in the middle zone, the 10-g mass significantly increased both GAG and collagen synthesis, and simultaneously promoted matrix reorganization via significantly increased collagen fibril density, alignment, and crosslinking, by 67%, 27%, 30%, 202%, and 263%, respectively, over all other loading levels. This enhanced matrix content and organization translated into significantly augmented tensile and compressive properties in the middle zone of 10-g-loaded constructs, which were found to be 3.5-, 3.7-, 2.1-, and 2.3-fold that of controls in terms of the E_Y, UTS, E_r, and E_i, respectively. Further, FEA found the 10-g mass to induce different strain gradients within each of the three axes of the neotissue's middle zone, with the *XX*-strain ranging from 5.7% to 10.1%, the *YY*-strain ranging from 7.2% to 18.3%, and the *ZZ*-strain ranging from -16.1% to -21.8%. Contrary to the initial hypothesis that a single strain threshold exists, these results suggest that separate strain thresholds may actually be necessary within the *XX*-, *YY*-, and *ZZ*-directions that together promote matrix synthesis and reorganization within the biconcave neotissue. Additionally, it was also found that 5 days of loading (from $t = 10$ to 14 days) were sufficient for the region-specific collagen fibril reorganization to be maintained throughout the remainder of the culture period, when no load was present. Together, these data suggest that exogenous strain applied early during neotissue development can be strategically fine-tuned to control lasting matrix synthesis and reorganization toward achieving improved functional properties in shape-specific neotissues.

Mechanical stimulation via axial loading enhanced the fibril alignment of the fibrocartilaginous neotissues in an anisotropic manner. FEA was conducted to understand how load influenced such alignment, finding the passive axial load-induced strains to be greatest in the middle zone of the biconcave model. This corroborates SEM results, which found the greatest tensile strain to occur in the *YY*-direction. This is physiologically significant, as the native TMJ disc presents with middle-zone matrix alignment in the same direction.[43] In terms of engineered tissues, similar correlations between loading direction and alignment have been observed in collagen gels in response to axial tensile strain[44] and in fibrin gels in response to axial compressive strain.[45] Such work has found increasing loading levels to correspond to increased alignment in the direction of loading. These previous studies, however, examined these effects in neotissues of uniform geometries, resulting in principally either tensile or compressive strains. The utility of a biconcave neotissue in the present study prompted the translation of a uniaxial load into multiaxial tensile and compressive strains. Thus, this study was able to promote region-specific alignment within the middle zone of the biconcave construct, leading to the development of functionally anisotropic neotissues.

Passive axial compressive loading was also found to promote matrix compaction and collagen crosslinking in the neotissue's middle zone. Specifically, this compaction and crosslinking was only observed at the 10-g loading level, where the neotissue had a significantly thinner and denser middle zone as well as increased PYR/WW and PYR/Col compared with all other groups. Previous work has found fiber alignment and compaction to go hand-in-hand; cell-seeded collagen gels have been found to undergo simultaneous fiber alignment and compaction in response to mechanical strain.[46–48] Further, treatment of cell-seeded collagen gels with sodium azide, an ATP inhibitor, or cytochalasin D, a cytoskeletal inhibitor, has been found to inhibit such matrix reorganization following mechanical stimulation.[49,50] Previous work has also correlated increased biomechanical properties in engineered neotissues with increased crosslinks,[38,51] suggesting that the greater functional properties in the middle zone of 10-g-loaded constructs are likely related to the increased crosslink content in this region. Such work indicates that cells, in response to a mechanical input, generate intrinsic traction forces to align compact, and crosslink collagen fibers such that they counter the newly loaded environment.[47] This, therefore, suggests that the strain-induced matrix changes observed in the self-assembled neotissue are primarily a cellular mechanotransductive response. In correlating cellular response to strain level, previous work has shown that anisotropic strains of ≥ 5–10% are necessary to induce fiber alignment and matrix compaction in cell-seeded collagen gels.[44,45] Results of the present study suggest that greater strain thresholds may be necessary to induce matrix reorganization in the self-assembled, biconcave neotissues. Specifically, only the 10-g mass, which promoted strains in the *XX*-, *YY*-, and *ZZ*-directions in excess of this 5–10% range in the neotissue middle zone, was found to align, compact, and crosslink the matrix.

To better understand how the strain-induced matrix reorganization influenced the functional properties of the biconcave neotissue, structure-function relationships were evaluated. Results of this analysis found significant, positive correlations between both collagen and GAG content with

FIG. 7. Structure-function correlations of neotissue middle-zone properties at $t = 5$ weeks. All correlations were found to be positive and statistically significant ($p < 0.05$). For the middle-zone compressive modulus, strong positive correlations ($R^2 > 0.5$) were found with PYR/Col, GAG/WW, and collagen fibril density, while weak positive correlations ($0 < R^2 < 0.5$) were found with collagen fibril alignment and Col/WW. For the middle-zone tensile modulus, strong positive correlations were found with collagen fibril alignment, PYR/Col, and Col/WW, while weak positive correlations were found with collagen fibril density and GAG/WW. Color images available online at www.liebertpub.com/tea

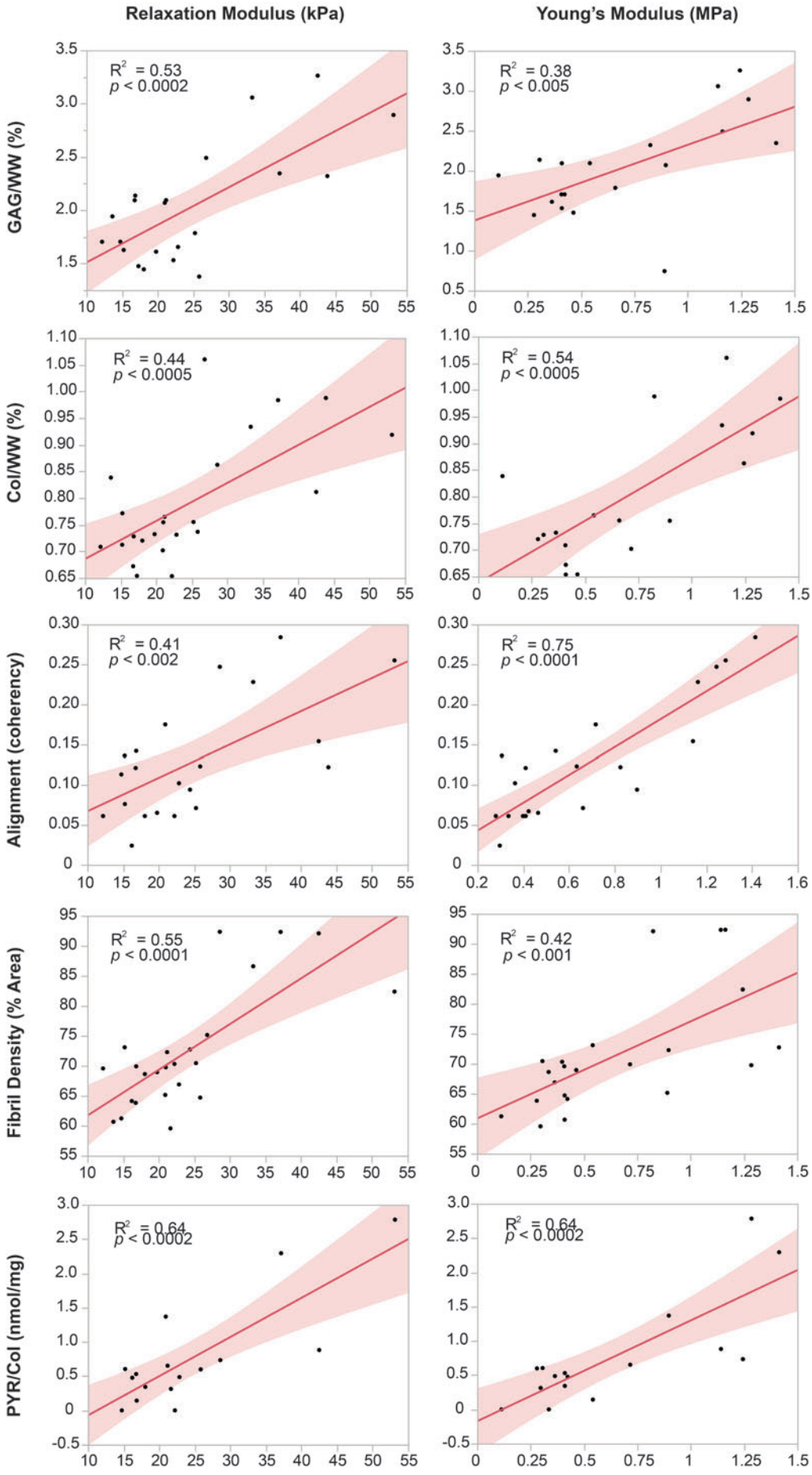
Relaxation Modulus (kPa)
Young's Modulus (MPa)
GAG/WW (%)
Col/WW (%)
Alignment (coherency)
Fibril Density (% Area)
PYR/Col (nmol/mg)
R² = 0.53
p < 0.0002
R² = 0.38
p < 0.005
R² = 0.44
p < 0.0005
R² = 0.54
p < 0.0005
R² = 0.41
p < 0.002
R² = 0.75
p < 0.0001
R² = 0.55
p < 0.0001
R² = 0.42
p < 0.001
R² = 0.64
p < 0.0002
R² = 0.64
p < 0.0002

both tensile and compressive properties, respectively. The strongest observed correlations for the tensile modulus were with collagen fibril alignment, PYR/Col, and collagen content. Positive, although weak, correlations were also found between the tensile stiffness modulus and both collagen density and GAG content. Previous work has shown that several types of proteoglycans, including dermatan sulfate and chondroitin sulfate, help regulate collagen fibrillogenesis and aid in microfibril aggregation to form a denser matrix, which may explain the positive correlations between GAG content and the tensile modulus.[52–54] In terms of the compressive properties, the strongest positive correlations were detected with PYR/Col, GAG content, and collagen fibril density, while weak positive correlations were found with both collagen content and alignment. Such findings support recent reports that likewise counter the traditionally accepted structure-function relationships of cartilaginous tissues, which correlated GAG content exclusively with compressive properties and collagen content with tensile properties.[55,56] Instead, it is now shown that a highly complex and integrated relationship appears to exist that connects not only overall matrix composition, but also its architecture with the functionality of both native and engineered cartilaginous tissues.[34,38,40,57–59] Gaining a better understanding of the intricate relationship between structure and function in engineered tissues should be the focus of future studies to aid in advancing tissue engineering endeavors.

Results of this study suggest that increased axial compressive loading may induce a more fibrocartilaginous matrix. Figure 3 shows denser, more uniform collagen type I staining in 10-g-loaded constructs compared with controls, while collagen type II staining appeared to decrease slightly with increasing load. Despite previous work that has linked compressive forces at the ligament–bone interface to induce collagen type II expression in tendon and ligaments, which typically express primarily collagen type I,[60,61] this study found compressive loading to instead increase collagen type I expression. Natively, fibrocartilaginous tissues face greater tensile strains compared with articular cartilage, therefore prompting the tissue to adapt to this unique environment.[17,62,63] As shown via FEA, the increased tensile and compressive strains in the different axes, which were found to correlate with fibril alignment, orientation, and compaction, may have likewise triggered collagen type I production in the neotissue middle zone. Other work has shown increased collagen type I expression and decreased collagen type II expression in canine intervertebral discs subjected to high axial compressive forces *in vivo*.[64] Similar to the present study, axial compressive loading has been predicted via FEA to translate into both tensile and compressive strains within the three-dimensional structure of the intervertebral disc.[65] Increased passive axial compressive loading levels, therefore, may have helped to drive the development of a more fibrocartilaginous engineered matrix expressing both collagen types I and II.[61,66] The present findings are very promising for fibrocartilage tissue engineering, as they suggest that tensile-compressive strains can be tailored to drive collagen production toward collagen type I, while decreasing collagen type II, resulting in a balance more on par with native tissue.

Previous work has highlighted the physiologic strain levels of cartilaginous tissues. Such work indicates that strains $\leq 20\%$ are within physiologic range for articular cartilage, whereas strains ≥ 40–60% are considered extreme and can lead to tissue degradation.[67,68] Similar strain levels have been predicted for both the meniscus and TMJ disc; FEA analysis has found tension-compression strain magnitudes in the range of ≥ 20–25% to correlate with normal physiologic loading.[69,70] Based on the present study's FEA analysis, it is predicted that the 10-g mass may be close to approaching an upper strain limit for passive axial compression, as maximum compressive strains in the *ZZ*-direction were found to be 21.8%. It is therefore important that future work determines whether higher passive axial loads are potentially more beneficial toward promoting enhanced functional properties in the biconcave neotissues and at which point the axial compression becomes detrimental. It has also been previously shown via single-cell studies that there is a ''critical strain threshold'' at $\sim 33\%$ applied axial compressive strain, at which point chondrocytes can no longer fully recover from the applied load.[71,72] Modeling work has further predicted that bulk tissue strains are $\sim 1.5\times$ higher within the microenvironment of the cells within loaded cartilaginous tissues.[73,74] This prior work, therefore, suggests that the cells within the biconcave constructs may be facing strains $\sim 1.5\times$ those applied to the tissue. Thus, future work should also consider the effects of passive axial loading on the cells comprising self-assembled neotissues, which may in turn help to infer upon both the local cellular- and tissue-level mechanical response of neotissues to axially applied strain.

Overall, this study suggests that passive axial compression, which represents a relatively simple and inexpensive means for inducing mechanical loading, is a promising tool for increasing the functional properties of engineered fibrocartilage. Not only does there appear to be a dose-dependent response to increased passive axial load, but strain thresholds also appear to exist in different directions above which matrix reorganization, synthesis, and collagen crosslinking become apparent. Overall, the neotissue developed in this study had GAG and compressive moduli on par with native tissue values; collagen content and tensile properties remained below native tissue values.[28] It should be noted that the focus of the present study was not to optimize matrix content; instead, the novelty of this work was using passive axial compressive loading as a means to tune matrix development and reorganization in an anisotropic manner, and, significantly, anisotropy was found to be conferred in a strain-dependent manner. Building upon this work, it is expected that future studies will combine higher levels of passive axial compressive loading with other classes of stimuli (e.g., soluble) to promote biochemical and biomechanical properties to levels seen in native tissues. It also remains to be seen how dynamic load stimulation could alter the matrix reorganization in the neotissue. Future studies should be conducted to determine the effects of passive axial loading on other shape-specific constructs, as this could lead to different strain distributions and, thus, neotissues having differential functional properties. Such work will greatly aid tissue engineers in their quest to drive *in vitro* neotissue development toward capturing the anisotropy and biomechanical complexity of musculoskeletal soft tissues, leading to neotissue implants of clinical relevance.

Acknowledgments

The authors would like to acknowledge funding support from NIH5-T32-GM008799 and R01 DEO19666.

Disclosure Statement

No competing financial interests exist.

References

1. Huey, D.J., Hu, J.C., and Athanasiou, K.A. Unlike bone, cartilage regeneration remains elusive. Science **338,** 917, 2012.
2. Almarza, A.J., and Athanasiou, K.A. Design characteristics for the tissue engineering of cartilaginous tissues. Ann Biomed Eng **32,** 2, 2004.
3. Buschmann, M.D., Gluzband, Y.A., Grodzinsky, A.J., and Hunziker, E.B. Mechanical compression modulates matrix biosynthesis in chondrocyte/agarose culture. J Cell Sci **108 (Pt 4),** 1497, 1995.
4. Hung, C.T., Mauck, R.L., Wang, C.C., Lima, E.G., and Ateshian, G.A. A paradigm for functional tissue engineering of articular cartilage via applied physiologic deformational loading. Ann Biomed Eng **32,** 35, 2004.
5. Hunter, C.J., Imler, S.M., Malaviya, P., Nerem, R.M., and Levenston, M.E. Mechanical compression alters gene expression and extracellular matrix synthesis by chondrocytes cultured in collagen I gels. Biomaterials **23,** 1249, 2002.
6. Vanderploeg, E.J., Imler, S.M., Brodkin, K.R., Garcia, A.J., and Levenston, M.E. Oscillatory tension differentially modulates matrix metabolism and cytoskeletal organization in chondrocytes and fibrochondrocytes. J Biomech **37,** 1941, 2004.
7. Ballyns, J.J., and Bonassar, L.J. Dynamic compressive loading of image-guided tissue engineered meniscal constructs. J Biomech **44,** 509, 2011.
8. Zhou, J., and Niklason, L.E. Microfluidic artificial ''vessels'' for dynamic mechanical stimulation of mesenchymal stem cells. Integr Biol (Camb) **4,** 1487, 2012.
9. Teh, T.K., Toh, S.L., and Goh, J.C. Aligned fibrous scaffolds for enhanced mechanoresponse and tenogenesis of mesenchymal stem cells. Tissue Eng Part A **19,** 1360, 2013.
10. Radlanski, R.J., and Renz, H. Genes, forces, and forms: mechanical aspects of prenatal craniofacial development. Dev Dyn **235,** 1219, 2006.
11. Meller, R., Schiborra, F., Brandes, G., Knobloch, K., Tschernig, T., Hankemeier, S., *et al.* Postnatal maturation of tendon, cruciate ligament, meniscus and articular cartilage: a histological study in sheep. Ann Anat **191,** 575, 2009.
12. Roddy, K.A., Prendergast, P.J., and Murphy, P. Mechanical influences on morphogenesis of the knee joint revealed through morphological, molecular and computational analysis of immobilised embryos. PLoS One **6,** e17526, 2011.
13. le Noble, F., Klein, C., Tintu, A., Pries, A., and Buschmann, I. Neural guidance molecules, tip cells, and mechanical factors in vascular development. Cardiovasc Res **78,** 232, 2008.
14. Responte, D.J., Lee, J.K., Hu, J.C., and Athanasiou, K.A. Biomechanics-driven chondrogenesis: from embryo to adult. FASEB J **26,** 3614, 2012.
15. Drury, J.L., and Mooney, D.J. Hydrogels for tissue engineering: scaffold design variables and applications. Biomaterials **24,** 4337, 2003.
16. Hodde, J. Naturally occurring scaffolds for soft tissue repair and regeneration. Tissue Eng **8,** 295, 2002.
17. Makris, E.A., Hadidi, P., and Athanasiou, K.A. The knee meniscus: structure-function, pathophysiology, current repair techniques, and prospects for regeneration. Biomaterials **32,** 7411, 2011.
18. Agrawal, C.M., Niederauer, G.G., and Athanasiou, K.A. Fabrication and Characterization of PLA-PGA Orthopedic Implants. Tissue Eng **1,** 241, 1995.
19. Bruns, J., Kahrs, J., Kampen, J., Behrens, P., Plitz, W. Autologous perichondral tissue for meniscal replacement. J Bone Joint Surg Br **80,** 918, 1998.
20. Puetzer, J.L., and Bonassar, L.J. High density type I collagen gels for tissue engineering of whole menisci. Acta Biomater **9,** 7787, 2013.
21. Wood, D.J., Minns, R.J., and Strover, A. Replacement of the rabbit medial meniscus with a polyester-carbon fibre bioprosthesis. Biomaterials **11,** 13, 1990.
22. Klompmaker, J., Veth, R.P., Jansen, H.W., Nielsen, H.K., de Groot, J.H., Pennings, A.J., *et al.* Meniscal repair by fibrocartilage in the dog: characterization of the repair tissue and the role of vascularity. Biomaterials **17,** 1685, 1996.
23. Agrawal, C.M., and Athanasiou, K.A. Technique to control pH in vicinity of biodegrading PLA-PGA implants. J Biomed Mater Res **38,** 105, 1997.
24. Hu, J.C., and Athanasiou, K.A. A self-assembling process in articular cartilage tissue engineering. Tissue Eng **12,** 969, 2006.
25. Hoben, G.M., Hu, J.C., James, R.A., and Athanasiou, K.A. Self-assembly of fibrochondrocytes and chondrocytes for tissue engineering of the knee meniscus. Tissue Eng **13,** 939, 2007.
26. Ofek, G., Revell, C.M., Hu, J.C., Allison, D.D., Grande-Allen, K.J., and Athanasiou, K.A. Matrix development in self-assembly of articular cartilage. PLoS One **3,** e2795, 2008.
27. Aufderheide, A.C., and Athanasiou, K.A. Assessment of a bovine co-culture, scaffold-free method for growing meniscus-shaped constructs. Tissue Eng **13,** 2195, 2007.
28. Macbarb, R.F., Chen, A.L., Hu, J.C., and Athanasiou, K.A. Engineering functional anisotropy in fibrocartilage neotissues. Biomaterials **34,** 9980, 2013.
29. Hirai, J., Kanda, K., Oka, T., and Matsuda, T. Highly oriented, tubular hybrid vascular tissue for a low pressure circulatory system. ASAIO J **40,** M383, 1994.
30. Hirai, J., and Matsuda, T. Self-organized, tubular hybrid vascular tissue composed of vascular cells and collagen for low-pressure-loaded venous system. Cell Transplant **4,** 597, 1995.
31. Huang, D., Chang, T.R., Aggarwal, A., Lee, R.C., and Ehrlich, H.P. Mechanisms and dynamics of mechanical strengthening in ligament-equivalent fibroblast-populated collagen matrices. Ann Biomed Eng **21,** 289, 1993.
32. L'Heureux, N., Germain, L., Labbe, R., and Auger, F.A. *In vitro* construction of a human blood vessel from cultured vascular cells: a morphologic study. J Vasc Surg **17,** 499, 1993.
33. L'Heureux, N., Paquet, S., Labbe, R., Germain, L., and Auger, F.A. A completely biological tissue-engineered human blood vessel. FASEB J **12,** 47, 1998.
34. MacBarb, R.F., Makris, E.A., Hu, J.C., and Athanasiou, K.A. A chondroitinase-ABC and TGF-beta1 treatment regimen for enhancing the mechanical properties of tissue-engineered fibrocartilage. Acta Biomater **9,** 4626, 2013.
35. Hu, J.C., and Athanasiou, K.A. The effects of intermittent hydrostatic pressure on self-assembled articular cartilage constructs. Tissue Eng **12,** 1337, 2006.

36. Huey, D.J., and Athanasiou, K.A. Tension-compression loading with chemical stimulation results in additive increases to functional properties of anatomic meniscal constructs. PLoS One **6,** e27857, 2011.
37. Natoli, R.M., Responte, D.J., Lu, B.Y., and Athanasiou, K.A. Effects of multiple chondroitinase ABC applications on tissue engineered articular cartilage. J Orthop Res **27,** 949, 2009.
38. Makris, E.A., MacBarb, R.F., Responte, D.J., Hu, J.C., and Athanasiou, K.A. A copper sulfate and hydroxylysine treatment regimen for enhancing collagen cross-linking and biomechanical properties in engineered neocartilage. FASEB J **27,** 2421, 2013.
39. Bank, R.A., Beekman, B., Verzijl, N., de Roos, J.A., Sakkee, A.N., and TeKoppele, J.M. Sensitive fluorimetric quantitation of pyridinium and pentosidine crosslinks in biological samples in a single high-performance liquid chromatographic run. J Chromatogr B Biomed Sci Appl **703,** 37, 1997.
40. Willard, V.P., Kalpakci, K.N., Reimer, A.J., and Athanasiou, K.A. The regional contribution of glycosaminoglycans to temporomandibular joint disc compressive properties. J Biomech Eng **134,** 011011, 2012.
41. Responte, D.J., Arzi, B., Natoli, R.M., Hu, J.C., and Athanasiou, K.A. Mechanisms underlying the synergistic enhancement of self-assembled neocartilage treated with chondroitinase-ABC and TGF-beta1. Biomaterials **33,** 3187, 2012.
42. Fonck, E., Feigl, G.G., Fasel, J., Sage, D., Unser, M., Rufenacht, D.A., *et al.* Effect of aging on elastin functionality in human cerebral arteries. Stroke **40,** 2552, 2009.
43. Scapino, R.P., Obrez, A., and Greising, D. Organization and function of the collagen fiber system in the human temporomandibular joint disk and its attachments. Cells Tissues Organs **182,** 201, 2006.
44. Vader, D., Kabla, A., Weitz, D., and Mahadevan, L. Strain-induced alignment in collagen gels. PLoS One **4,** e5902, 2009.
45. Girton, T.S., Barocas, V.H., and Tranquillo, R.T. Confined compression of a tissue-equivalent: collagen fibril and cell alignment in response to anisotropic strain. J Biomech Eng **124,** 568, 2002.
46. Grinnell, F. Fibroblast-collagen-matrix contraction: growth-factor signalling and mechanical loading. Trends Cell Biol **10,** 362, 2000.
47. Harris, A.K., Stopak, D., and Wild, P. Fibroblast traction as a mechanism for collagen morphogenesis. Nature **290,** 249, 1981.
48. Tranquillo, R.T. Self-organization of tissue-equivalents: the nature and role of contact guidance. Biochem Soc Symp **65,** 27, 1999.
49. Grenier, G., Remy-Zolghadri, M., Larouche, D., Gauvin, R., Baker, K., Bergeron, F., *et al.* Tissue reorganization in response to mechanical load increases functionality. Tissue Eng **11,** 90, 2005.
50. Canty, E.G., Starborg, T., Lu, Y., Humphries, S.M., Holmes, D.F., Meadows, R.S., *et al.* Actin filaments are required for fibripositor-mediated collagen fibril alignment in tendon. J Biol Chem **281,** 38592, 2006.
51. Makris, E.A., Hu, J.C., and Athanasiou, K.A. Hypoxia-induced collagen crosslinking as a mechanism for enhancing mechanical properties of engineered articular cartilage. Osteoarthritis Cartilage **21,** 634, 2013.
52. Scott, J.E., Orford, C.R., and Hughes, E.W. Proteoglycan-collagen arrangements in developing rat tail tendon. An electron microscopical and biochemical investigation. Biochem J **195,** 573, 1981.
53. Chandrasekhar, S., Kleinman, H.K., Hassell, J.R., Martin, G.R., Termine, J.D., and Trelstad, R.L. Regulation of type I collagen fibril assembly by link protein and proteoglycans. Coll Relat Res **4,** 323, 1984.
54. Snowden, J.M., and Swann, D.A. Effects of glycosaminoglycans and proteoglycan on the *in vitro* assembly and thermal stability of collagen fibrils. Biopolymers **19,** 767, 1980.
55. Chia, H.N., and Hull, M.L. Compressive moduli of the human medial meniscus in the axial and radial directions at equilibrium and at a physiological strain rate. J Orthop Res **26,** 951, 2008.
56. Recuerda, M., Cote, S.P., Villemure, I., and Perie, D. Influence of experimental protocols on the mechanical properties of the intervertebral disc in unconfined compression. J Biomech Eng **133,** 071006, 2011.
57. Nerurkar, N.L., Han, W., Mauck, R.L., and Elliott, D.M. Homologous structure-function relationships between native fibrocartilage and tissue engineered from MSC-seeded nanofibrous scaffolds. Biomaterials **32,** 461, 2011.
58. Khalsa, P.S., and Eisenberg, S.R. Compressive behavior of articular cartilage is not completely explained by proteoglycan osmotic pressure. J Biomech **30,** 589, 1997.
59. Allen, K.D., and Athanasiou, K.A. A surface-regional and freeze-thaw characterization of the porcine temporomandibular joint disc. Ann Biomed Eng **33,** 951, 2005.
60. Sagarriga Visconti, C., Kavalkovich, K., Wu, J., and Niyibizi, C. Biochemical analysis of collagens at the ligament-bone interface reveals presence of cartilage-specific collagens. Arch Biochem Biophys **328,** 135, 1996.
61. Benjamin, M., and Ralphs, J.R. Fibrocartilage in tendons and ligaments—an adaptation to compressive load. J Anat **193 (Pt 4),** 481, 1998.
62. Freeman, P.M., Natarajan, R.N., Kimura, J.H., and Andriacchi, T.P. Chondrocyte cells respond mechanically to compressive loads. J Orthop Res **12,** 311, 1994.
63. Giori, N.J., Beaupre, G.S., and Carter, D.R. Cellular shape and pressure may mediate mechanical control of tissue composition in tendons. J Orthop Res **11,** 581, 1993.
64. Hutton, W.C., Toribatake, Y., Elmer, W.A., Ganey, T.M., Tomita, K., and Whitesides, T.E. The effect of compressive force applied to the intervertebral disc *in vivo*. A study of proteoglycans and collagen. Spine (Phila Pa 1976) **23,** 2524, 1998.
65. Shirazi-Adl, S.A., Shrivastava, S.C., and Ahmed, A.M. Stress analysis of the lumbar disc-body unit in compression. A three-dimensional nonlinear finite element study. Spine (Phila Pa 1976) **9,** 120, 1984.
66. Hoben, G.M., and Athanasiou, K.A. Creating a spectrum of fibrocartilages through different cell sources and biochemical stimuli. Biotechnol Bioeng **100,** 587, 2008.
67. Armstrong, C.G., Bahrani, A.S., and Gardner, D.L. Changes in the deformational behavior of human hip cartilage with age. J Biomech Eng **102,** 214, 1980.
68. Herberhold, C., Faber, S., Stammberger, T., Steinlechner, M., Putz, R., Englmeier, K.H., *et al. In situ* measurement of articular cartilage deformation in intact femoropatellar joints under static loading. J Biomech **32,** 1287, 1999.
69. Spilker, R.L., Donzelli, P.S., and Mow, V.C. A transversely isotropic biphasic finite element model of the meniscus. J Biomech **25,** 1027, 1992.

70. Spilker, R.L., Nickel, J.C., and Iwasaki, L.R. A biphasic finite element model of *in vitro* plowing tests of the temporomandibular joint disc. Ann Biomed Eng **37,** 1152, 2009.
71. Ofek, G., Wiltz, D.C., and Athanasiou, K.A. Contribution of the cytoskeleton to the compressive properties and recovery behavior of single cells. Biophys J **97,** 1873, 2009.
72. Shieh, A.C., Koay, E.J., and Athanasiou, K.A. Strain-dependent recovery behavior of single chondrocytes. Biomech Model Mechanobiol **5,** 172, 2006.
73. Guilak, F., and Mow, V.C. The mechanical environment of the chondrocyte: a biphasic finite element model of cell-matrix interactions in articular cartilage. J Biomech **33,** 1663, 2000.
74. Guilak, F., Ratcliffe, A., and Mow, V.C. Chondrocyte deformation and local tissue strain in articular cartilage: a confocal microscopy study. J Orthop Res **13,** 410, 1995.

Address correspondence to:
Kyriacos A. Athanasiou, PhD, PE
Department of Biomedical Engineering
University of California, Davis
One Shields Avenue
Davis, CA 95616

E-mail: athanasiou@ucdavis.edu

Received: November 8, 2013
Accepted: May 29, 2014
Online Publication Date: July 18, 2014